

The following publication Y. Yang, S. Tan and S. Y. R. Hui, "Front-End Parameter Monitoring Method Based on Two-Layer Adaptive Differential Evolution for SS-Compensated Wireless Power Transfer Systems," in IEEE Transactions on Industrial Informatics, vol. 15, no. 11, pp. 6101-6113, Nov. 2019 is available at <https://doi.org/10.1109/TII.2019.2924926>

Front-End Parameter Monitoring Method Based on Two-Layer Adaptive Differential Evolution For SS-Compensated Wireless Power Transfer Systems

Yun Yang, *Member, IEEE*, Siew-Chong Tan, *Senior Member, IEEE*, and Shu Yuen Ron Hui, *Fellow, IEEE*

Abstract—In this paper, a two-layer adaptive Differential Evolution (ADE) algorithm is adopted to monitor the parameters of the receiving resonators and the mutual inductances of series-series (SS)-compensated wireless power transfer (WPT) systems. By only measuring the primary coils' voltages and currents, the proposed monitoring method can be applied for multiple-coil SS-compensated WPT systems without any feedback signals from the receivers. Compared to the conventional monitoring method based on the Genetic Algorithm (GA), which may find local optimal solutions by the manually tuned parameters of the mutation rate, the crossover rate, and the generations, the proposed method based on the two-layer ADE can always find global optimal solutions by the automatically tuned parameters of the differential weight, the crossover rate, and the generations. Experimental results validate that the ADE and the proposed two-layer ADE can monitor the parameters of both two- and three-coil SS-compensated WPT systems more steadily and accurately than the conventional GA. Additionally, the proposed two-layer ADE is verified to monitor the parameters of three-coil SS-compensated WPT systems with three different arrangements more accurately than the ADE.

Index Terms—Parameter monitoring, series-series (SS)-compensated wireless power transfer (WPT) system, Genetic Algorithm (GA), adaptive Differential Evolution (ADE), two-layer ADE.

ABBREVIATION AND NOMENCLATURE

WPT	Wireless power transfer
EV	Electric vehicle
SS	Series-series
SP	Series-parallel
PP	Parallel-parallel
PS	Parallel-series
GA	Genetic algorithm
DE	Differential evolution

Manuscript received January 21, 2019; revised March 11, 2019; accepted June 20, 2019. This work is supported by the Hong Kong Research Grant Council under Theme-based Research Project: T23-701/14-N.

Y. Yang and S. C. Tan are with the Department of Electrical and Electronic Engineering, The University of Hong Kong, Hong Kong (e-mail: cacalotoyangyun@gmail.com, sctan@eee.hku.hk).

S. Y. R. Hui is with the Department of Electrical and Electronic Engineering, The University of Hong Kong, Hong Kong and also with the Department of Electrical and Electronic Engineering, Imperial College London, London SW7 2AZ, U.K. (e-mail: ronhui@eee.hku.hk).

ADE	Adaptive differential evolution
DC	Direct current
AC	Alternative current
ESR	Equivalent series resistance
DSP	Digital signal processor
L_p	Inductance of the transmitting coil
C_p	Capacitance of the compensated capacitor of the transmitting coil
R_p	ESR of the transmitting coil
L_{si}	Inductances of the receiving coils
C_{si}	Capacitances of the compensated capacitors of the receiving coils
R_{si}	ESRs of the receiving coils
R_{L_i}	Load resistances
M_i	Mutual inductances between the transmitting coil and the receiving coils
M_{ij}	Mutual inductances between the receiving coils
R_{eq1i}	ESRs of the receiving resonators
Z_{p1l}	Equivalent impedance of the WPT system at the fundamental frequency
ω_l	Switching angular frequency
ω_o	Resonant switching angular frequency
$\omega_L, L_{siL}, C_{siL}, R_{eq1L}, M_{iL}, M_{ijL}$	Lower bounds of $\omega_l, L_{si}, C_{si}, R_{eq1i}, M_i, M_{ij}$
$\omega_H, L_{siH}, C_{siH}, R_{eq1H}, M_{iH}, M_{ijH}$	Upper bounds of $\omega_l, L_{si}, C_{si}, R_{eq1i}, M_i, M_{ij}$
P_{size}	Population size of the heuristic algorithms
C_{size}	Number of bits in each chromosome of GA
max_{gen}	Maximum generations of the heuristic algorithms
P_c	Crossover rate of GA
P_m	Mutual rate of GA
$X_{pi}(g)$	Randomly selected vectors of ADE and the two-layer ADE
F_a	Adaptive differential weight of ADE and the two-layer ADE
F_{low}	Lower bound of the adaptive differential weight
F_{up}	Upper bound of the adaptive differential weight
f_a	Fitness of the individual α
f_{min}	Minimum fitness
f_{max}	Maximum fitness
f_{ave}	Averaged fitness
$H_a(g)$	Yield of offspring
P_{ca}	Crossover rate of ADE and the two-layer ADE

P_{low}	Lower bound of the crossover rate
P_{up}	Upper bound of the crossover rate
r_{α}	A random number for the individual α
R_{α}	A random index for dimensionality
ζ	Damping ratio of the second-order bandpass filter
D	Distance between the coils
nvar	Number of the monitored variables

I. INTRODUCTION

EVER since the two coil nonradiative WPT system was first reported by Nicola Tesla in 1914 [1], the WPT technique based on the near-field magnetic coupling has been broadly applied in medical implants [2]–[4], EVs [5]–[7], induction heaters [8], and wireless cell phone chargers [9]–[14]. All these applications adopt Tesla’s principle to compensate the leakage inductance in the power flow path and to ensure good transmission efficiency by various compensation topologies, which include SS, SP, PP, PS, and hybrid compensations [15]. Among them, the SS-compensation is widely adopted for its design being independent of load and coupling coefficient [16].

In recent years, research activities to improve the controllability, transmission efficiencies and dynamic performances of SS-compensated WPT systems are intensified [17]–[24]. Accurate values of the parameters, including mutual inductances, impedances of the receiving resonators, and load conditions, are usually required for the controllers of SS-compensated WPT systems to achieve optimal efficiency operations and better dynamic performances. For instance, real-time mutual coupling conditions are needed for the optimal efficiency operations of the WPT system with movable loads [25]. Load conditions are needed for the nonlinear control of the WPT system to reduce the overshoot/undershoot of the output voltage [26]. Therefore, accurate online monitoring of the parameters can prevent the transmission efficiency and the dynamic performance of an SS-compensated WPT system being deteriorated by the variations of operating conditions.

Besides, front-end parameter monitoring can also (i) reduce the complexity and costs of communication devices that are often adopted in WPT systems for feedback control [27], [28]; (ii) detect the ageing effect of receiving coils and loads by monitoring their equivalent resistances. By far, several front-end parameter monitoring methods have been proposed to replace the communication channels of SS-compensated WPT systems to achieve the optimal operations [29]–[34]. In [29], an envelope detector and a phase detector are used to extract the required information of the transmitting current to estimate the load resistance. In [30], a transient model of a SS-compensated WPT system is used to detect the initial load condition by injecting a series of high-frequency signals before startup. In [31] and [32], both the load resistance and the coupling coefficient can be uniquely determined by measuring the input voltage and the current at only one frequency. In [33], a computation-based estimation strategy for the load impedances and the coupling coefficients of a SS-compensated WPT system with two loads is demonstrated. These pioneering strategies are primarily designed to monitor the load impedances and the coupling coefficients of SS-compensated

WPT systems, whereas few of them monitor the parameters of the resonant tanks. As a matter of fact, most of these strategies are designed based on the known values of the parameters of the resonant tanks, which is impractical as the front-end users are unlikely to measure such parameters. The mutual inductance values are highly sensitive to the coils’ dimensions, locations and orientations. Particularly for the SS-compensated WPT systems with multiple coils, any slight change in the distances and orientations of the coils can lead to significant errors in the mutual inductance values. Besides, the inductances of the coils and the capacitances of the compensated capacitors are usually close but not exactly equal to the rated values. Consequently, using nominal values of the parameters can lead to inaccurate prediction of optimal operations. Therefore, accurate online monitoring of the parameters is critical. In [34], a front-end parameter monitoring method based on the conventional GA is presented to identify the compensated capacitances and the distances between the coils. The proposed method avoids the requirement of prior knowledge of all parameter measurements and overcomes the component tolerance issue. The method based on the heuristic algorithm can find optimal solutions more efficiently than the traditional optimization methods (e.g. linear programming) for complex systems with multiple variables [35]. However, conventional GA has the risk of being trapped in local optimal points. Thus, unsteady performances with strong randomness can always occur when the number of iterations increases [36]. Besides, various parameters of the conventional GA, including the crossover rate, the mutation rate, and the generations, are difficult to tune [37]. Thus, the method in [34] requires rich experience in tuning the parameter selection ranges and designs of constraints and objective functions for SS-compensated WPT systems.

DE is a simple, yet powerful evolutionary algorithm developed by Storn and Price for continuous space optimization. It can find global optimal solutions with a faster and smoother convergence, as compared to the algorithms of the adaptive Simulated Annealing and the Nelder-Mead method [38]. More importantly, DE has shown to outperform conventional GA regarding numerous single-objective and multi-objective problems in different areas [39]–[44]. Based on the DE, the ADE with the adaptive differential weight and the crossover rate is further proposed by the evaluations of 24 benchmark functions [45]. Compared to the conventional GA, the ADE can obviously exhibit more efficient explorations in the decision space. In this paper, based on the ADE, a two-layer ADE is designed and applied to monitor the parameters of the receiving resonators and the mutual inductances of SS-compensated WPT systems. The primary layer is to monitor the coil inductances and the compensated capacitances of the receiving resonators. Then, based on the identified coil inductances and the compensated capacitances of the receiving resonators, the secondary layer is to monitor the equivalent resistances of the receiving resonators and the mutual inductances. The motivation of designing the two-layer ADE is that the ADE can accurately monitor the coil inductances and the compensated capacitances of the receiving resonators but may fail to monitor the equivalent resistances of the receiving resonators and the mutual inductances for multiple-coil WPT systems. This is due to the high randomness of the monitored

parameters for the ADE. As a result, the identified values of the dominant parameters vary negligibly while the identified values of the minor parameters vary significantly. To this end, the major parameters of the coil inductances and the compensated capacitors of the receiving resonators are initially identified as the known parameters. The randomness of the monitored parameters is reduced by halving the number of the monitored parameters. Then, the minor parameters can be accurately monitored based on the objective function of the secondary-layer of the two-layer ADE. The two-layer ADE monitor the parameters more accurately than the ADE. Compare the two-layer ADE to the conventional GA, stabilities and accuracies of the monitoring are significantly improved.

The proposed front-end parameter monitoring method based on the heuristic algorithm of ADE or the two-layer ADE, to the best of our knowledge, has not been investigated. Compared to the conventional method based on GA to monitor the compensated capacitances in [34] and the method based on estimation equations to monitor the mutual inductances and load conditions in [31]–[33], the proposed method can simultaneously monitor the mutual inductances, the load conditions, and the parameters of receiving resonators. Besides, the proposed method can be used to monitor the parameters of two identical receiving coils located symmetrically with respect to the transmitting coil, which is invalidated for the conventional method using least square approximation [33].

II. DERIVATIONS OF THE IDENTIFICATION MODEL

A typical SS-compensated WPT system with multiple outputs is shown in Fig. 1. At the transmitting side, a full-bridge inverter is controlled by a phase shift control with the fixed duty ratio of 0.5 to convert the DC voltage source V_{dc} to a high-frequency alternating voltage v_p . The transmitting resonator comprises a coil with the inductance of L_p , a compensated capacitor with the capacitance of C_p , and their ESR of R_p . At the receiving sides, the receiving resonators comprise the coil inductances of L_{si} ($i=1, 2, \dots, m$), compensated capacitances of C_{si} ($i=1, 2, \dots, m$), their ESRs of R_{si} ($i=1, 2, \dots, m$), and the load resistances R_{Li} ($i=1, 2, \dots, m$). Here, the resistive load can be an AC load or an equivalent load of a diode bridge rectifier and a DC load [22]. M_i ($i=1, 2, \dots, m$) are the mutual inductances between the transmitting coil and the receiving coils. M_{ij} ($i=1, 2, \dots, m, j=1, 2, \dots, m, i \neq j$) are the mutual inductances between the receiving coils.

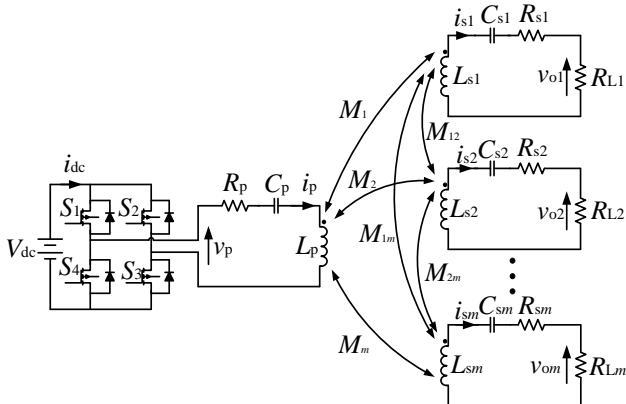


Fig. 1. Topology of an SS-compensated WPT system with multiple outputs.

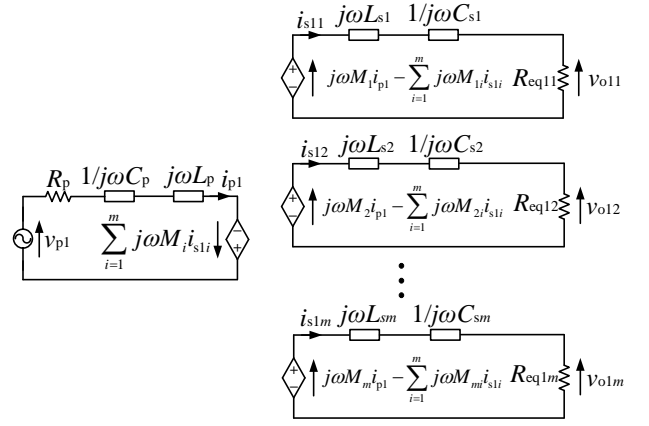


Fig. 2. Equivalent circuit of an SS-compensated WPT system at the fundamental frequency with multiple outputs.

The input voltage of the transmitting resonator v_p is generally pulse or pseudo-pulse waveforms, which contain plentiful odd-harmonics. For the currents of both resonators i_p and i_{si} ($i=1, 2, \dots, m$), high-order odd-harmonics may also exist at some operating conditions. Hence, to simplify the analysis, the equivalent circuit of a multiple-coil SS-compensated WPT system at the fundamental frequency can be depicted by decoupling the parameters of v_p , v_{oi} , i_p , and i_{si} ($i=1, 2, \dots, m$) into the respective harmonics, as shown in Fig. 2. Here, v_{p1} , v_{o1i} , i_{p1} , and i_{s1i} are fundamental components. R_{eq1i} ($i=1, 2, \dots, m$) are the equivalent resistances of the receiving resonators, R_{eq1i} . Besides, the “self-mutual inductances” are physically null (i.e. $M_{11}=M_{22}=\dots=M_{mm}=0$). Based on the equivalent circuit in Fig. 2,

$$\begin{cases} v_{p1} = \left[R_p + \left(\omega L_p - \frac{1}{\omega C_p} \right) j \right] i_{p1} - \omega \mathbf{M}^T \mathbf{i}_{s1} j \\ \omega \mathbf{M} i_{p1} j - \omega \mathbf{M}_1 \mathbf{i}_{s1} j = \mathbf{Z}_s \mathbf{i}_{s1} \end{cases} \quad (1)$$

where $\mathbf{i}_{s1} = [i_{s11}, i_{s12}, \dots, i_{s1m}]^T$, $\mathbf{M} = [M_1, M_2, \dots, M_m]^T$, $\mathbf{M}_1 = \begin{bmatrix} 0 & M_{12} & \dots & M_{1m} \\ M_{21} & 0 & \dots & M_{2m} \\ \vdots & \vdots & \ddots & \vdots \\ M_{m1} & M_{m2} & \dots & 0 \end{bmatrix}$, $\mathbf{Z}_s = \begin{bmatrix} Z_{s1} & 0 & \dots & 0 \\ 0 & Z_{s2} & \dots & 0 \\ \vdots & \vdots & \ddots & \vdots \\ 0 & 0 & \dots & Z_{sm} \end{bmatrix}$, and $Z_{si} = R_{eq1i} + \left(\omega L_{si} - \frac{1}{\omega C_{si}} \right) j$ ($i=1, 2, \dots, m$).

Simplify (1) by cancelling the term \mathbf{i}_{s1} ,

$$\frac{v_{p1}}{i_{p1}} = Z_{p1} = R_p + \left(\omega L_p - \frac{1}{\omega C_p} \right) j + \omega^2 \mathbf{M}^T (\omega \mathbf{M}_1 j + \mathbf{Z}_s)^{-1} \mathbf{M} \quad (2.1)$$

where Z_{p1} is the equivalent impedance of the SS-compensated WPT system at the fundamental frequency. By rearranging (2.1) by separating the real and imaginary parts,

$$\begin{aligned} \frac{v_{p1}}{i_{p1}} = \mathbf{Re}(Z_{p1}) + \mathbf{Im}(Z_{p1}) = & \left(R_p + \omega^2 P(\mathbf{M}, \mathbf{M}_1, \mathbf{Z}_s, \omega) \right) + \\ & \left(\omega L_p - \frac{1}{\omega C_p} + \omega^2 Q(\mathbf{M}, \mathbf{M}_1, \mathbf{Z}_s, \omega) \right) j \end{aligned} \quad (2.2)$$

where the real and imaginary parts of Z_{p1} are

$$\mathbf{Re}(Z_{p1}) = R_p + \omega^2 P(\mathbf{M}, \mathbf{M}_1, \mathbf{Z}_s, \omega) \quad (2.3)$$

$$\mathbf{Im}(Z_{p1}) = \left(\omega L_p - \frac{1}{\omega C_p} + \omega^2 Q(\mathbf{M}, \mathbf{M}_1, \mathbf{Z}_s, \omega) \right) j \quad (2.4)$$

$P(\mathbf{M}, \mathbf{M}_1, \mathbf{Z}_s, \omega)$ and $Q(\mathbf{M}, \mathbf{M}_1, \mathbf{Z}_s, \omega)$ are scalars, which are determined by the values of \mathbf{M} , \mathbf{M}_1 , \mathbf{Z}_s and ω . Theoretically, the

values of \mathbf{M} , \mathbf{M}_1 and \mathbf{Z}_s can be obtained by numbers of v_{p1} and i_{p1} being measured at different ω . In other words, the equivalent impedance Z_{p1} of the SS-compensated WPT system at the fundamental frequency varies by sweeping the switching angular frequency ω from the lower bound ω_L to the upper bound ω_H . The equivalent impedance Z_{p1} depends on the parameters of L_p , C_p , R_p , L_{si} , C_{si} , R_{eq1i} , \mathbf{M} , and \mathbf{M}_1 ,

$$\begin{cases} \frac{v_{p1}}{i_{p1}} = Z_{p1} = f(L_p, C_p, R_p, L_{si}, C_{si}, R_{eq1i}, \mathbf{M}, \mathbf{M}_1, \omega_l) \\ \omega_L \leq \omega_l \leq \omega_H \end{cases}, \quad (3)$$

where n is the number of the measured v_{p1} and i_{p1} for the monitoring. With practical considerations, L_p , C_p and R_p of the transmitting coil are preliminarily known parameters. Then, the identification model for the parameters of the receiving resonators and the mutual inductances can be derived as

$$\min J = \|\mathbf{v}_{p1est} - \mathbf{v}_{p1}\| \quad (4)$$

s.t. $\mathbf{v}_{p1est} = \mathbf{i}_{p1} \mathbf{Z}_{p1}$, $\omega_L \leq \omega_l \leq \omega_H$, $L_{siL} \leq L_{si} \leq L_{siH}$, $C_{siL} \leq C_{si} \leq C_{siH}$, $R_{eq1iL} \leq R_{eq1i} \leq R_{eq1iH}$, $\mathbf{M}_L \leq \mathbf{M} \leq \mathbf{M}_H$, and $\mathbf{M}_{1L} \leq \mathbf{M}_1 \leq \mathbf{M}_{1H}$ ($i = 1, 2, \dots, m$) ($j = 1, 2, \dots, n$), where

$$\mathbf{Z}_{p1} = \begin{bmatrix} Z_{p11} & 0 & \dots & 0 \\ 0 & Z_{p12} & \dots & 0 \\ \vdots & \vdots & \ddots & \vdots \\ 0 & 0 & \dots & Z_{p1m} \end{bmatrix}. \text{ The estimated input voltages of}$$

the transmitting resonator $\mathbf{v}_{p1est} = [v_{p1est1}, v_{p1est2}, \dots, v_{p1estm}]$ are calculated by the equation $\mathbf{v}_{p1est} = \mathbf{i}_{p1} \mathbf{Z}_{p1}$ based on the measured transmitting currents $\mathbf{i}_{p1} = [i_{p11}, i_{p12}, \dots, i_{p1n}]$ and the searching parameters of L_{si} , C_{si} , R_{eq1i} , \mathbf{M} , and \mathbf{M}_1 at the switching angular frequencies ω_l ($l = 1, 2, \dots, n$). The expressions of Z_{p1l} are given in (2). The objective of the identification model is to minimize the norm of the voltage differences between the estimated input voltages \mathbf{v}_{p1est} and the measured input voltages \mathbf{v}_{p1} . The identified parameters L_{si} , C_{si} , R_{eq1i} , \mathbf{M} , and \mathbf{M}_1 are searched within the lower bounds of L_{siL} , C_{siL} , R_{eq1iL} , \mathbf{M}_L , \mathbf{M}_{1L} and the upper bounds of L_{siH} , C_{siH} , R_{eq1iH} , \mathbf{M}_H , \mathbf{M}_{1H} . The values of the bounds are determined empirically.

III. DESCRIPTIONS OF THE ALGORITHMS

Based on the identification model, three evolutionary algorithms, including the conventional GA, the ADE, and the proposed two-layer ADE are adopted in this paper to minimize the objective function in (4), thus monitoring the parameters of the receiving resonators and the mutual inductances.

A. Brief Reviews of the Conventional GA

For the conventional GA [34], the individuals, being encoded in strings of bits (0s and 1s), also known as the chromosomes, are randomly generated for each parameter (L_{si} , C_{si} , R_{eq1i} , \mathbf{M} , and \mathbf{M}_1) with the population size of P_{size} initially. Each chromosome contains C_{size} bits. Then, by decoding the binary chromosomes into the decimal solutions, the objective function $J = \|\mathbf{v}_{p1est} - \mathbf{v}_{p1}\|$ can be evaluated based on the decimal individuals. If either of the terminal conditions of (i) the generations reaching the maximum generations max_{gen} or (ii) the algorithm being convergent, is satisfied, the algorithm stops and output the optimum solutions and the corresponding fitness value. On the contrary, if none of the terminal conditions is satisfied, the algorithm goes to the operations of selection, crossover, and mutation. For the selection operation, first two

parent chromosomes in the current population are selected based on the sorted fitness (greater opportunities to be selected in the roulette for smaller fitness). For the crossover operation, two selected parent chromosomes cross over at every two loci (positions in two chromosomes) to generate an offspring with the crossover rate of P_c . If no crossover operation is performed, the parent chromosomes are copied. For the mutation operation, the new offspring mutates at each locus (position in the chromosome) to generate another offspring with the mutation rate of P_m . If no mutation operation is performed, the parent chromosome is copied. Then, the newly generated population is applied for the next iteration.

B. ADE

The process of the ADE algorithm can be described in detail as follows: **[Initialization]** Generate a random population of P_{size} individuals in the search-space (within the lower and the upper bounds in (4)) for the parameters of L_{si} , C_{si} , R_{eq1i} , \mathbf{M} , and \mathbf{M}_1 . **[Fitness]** Evaluate the fitness of each individual using the objective function $J = \|\mathbf{v}_{p1est} - \mathbf{v}_{p1}\|$. **[Checked]** If both the termination conditions of (i) generations reaching the maximum generations max_{gen} and (ii) the algorithm being convergent, are satisfied, the algorithm stops and output the optimum solutions and the corresponding fitness value. On the contrary, if any one of the termination conditions is not satisfied, the algorithm repeats in the adaptive mutation operation, the adaptive crossover operation, and the selection operation. **[New population] Create a new population by repeating the following steps:** i) Adaptive mutation operation: Randomly select three vectors of $X_{p1}(g)$, $X_{p2}(g)$, and $X_{p3}(g)$ with distinct indices of p_1 , p_2 , p_3 , where g indicates the number of the iterations. Then, apply the three vectors into the adaptive function

$$F_\alpha = F_{low} + (F_{up} - F_{low}) \frac{f_2 - f_1}{f_3 - f_1}, \quad (5)$$

where F_α is the adaptive differential weight; F_{low} and F_{up} are the lower and upper bounds of the differential weight, respectively; f_1, f_2 , and f_3 are the fitness of $X_{p1}(g)$, $X_{p2}(g)$, and $X_{p3}(g)$, $f_1 < f_2 < f_3$. Consequently, a new offspring using the differential strategies of DE/rand/1 (mutation operators are based on randomly chosen base vectors and one vector difference is used) can be obtained as

$$H_\alpha(g) = X_{p1}(g) + F_\alpha (X_{p2}(g) - X_{p3}(g)), \quad (6)$$

where $H_\alpha(g)$ is the yield of offspring. If $H_\alpha(g)$ is invalid, the adaptive mutation operation needs to be performed again until it is in the search-space. ii) Adaptive crossover operation: Cross over the two selected parents to generate a new offspring $H_\alpha(g)$ with the crossover rate P_{ca} ,

$$P_{ca} = \begin{cases} P_{low} + \frac{(P_{up} - P_{low})(f_\alpha - f_{min})}{(f_{max} - f_{min})} & f_\alpha < f_{ave} \\ P_{low} & f_\alpha \geq f_{ave} \end{cases}, \quad (7)$$

where P_{low} and P_{up} are the lower and upper bounds of the crossover rate; f_α is the fitness of the individual α ; f_{min} and f_{max} are the minimum and the maximum fitness; f_{ave} is the averaged fitness. If $r_\alpha < P_{ca}$ or $\alpha = R_\alpha$, where r_α is a random number; R_α is a random index for dimensionality, then set $H_\alpha(g) = X_{p1}(g) + F_\alpha (X_{p2}(g) - X_{p3}(g))$. If no crossover operation is performed,

the parents are copied. (3) Selection operation: Compare $J(X_{\alpha+1})$ to $J(X_\alpha)$. If $J(X_{\alpha+1}) < J(X_\alpha)$, then replace the solution in the current population by the improved candidate solution $X_{\alpha+1}$ based on the greedy selection method. **[Replace and loop]** If the termination conditions are not satisfied, the algorithm goes to the operations of the adaptive mutation, adaptive crossover, and selection, to generate a new population for a further run.

C. Proposed Two-Layer ADE

Compared to the ADE, the proposed two-layer ADE checks the termination conditions twice. As shown in Fig. 3, the dominant parameters of the coil inductances L_{si} and the compensated capacitances C_{si} of the receiving resonators are primarily identified in the primary layer when the first terminated conditions are satisfied. Then, the identified parameters L_{si} and C_{si} are considered to be known parameters, such that the identification model for the secondary layer is

$$\min J = \|\mathbf{i}_{p1est} - \mathbf{i}_{p1}\| \quad (8)$$

s.t. $\mathbf{i}_{p1est} = \mathbf{v}_{p1}/\mathbf{Z}_{p1}$, $\omega_L \leq \omega_l \leq \omega_H$, $R_{eq1iL} \leq R_{eq1i} \leq R_{eq1iH}$, $\mathbf{M}_L \leq \mathbf{M} \leq \mathbf{M}_H$, and $\mathbf{M}_{1L} \leq \mathbf{M}_1 \leq \mathbf{M}_{1H}$ ($i = 1, 2, \dots, m$) ($j = 1, 2, \dots, n$), where the estimated currents of the transmitting resonator $\mathbf{i}_{p1est} = [i_{p1est1}, i_{p1est2}, \dots, i_{p1estn}]$ are calculated by the equation $\mathbf{i}_{p1est} = \mathbf{v}_{p1}/\mathbf{Z}_{p1}$ based on the measured input voltages $\mathbf{v}_{p1} = [v_{p11}, v_{p12}, \dots, v_{p1n}]$ and the searching parameters of R_{eq1i} , \mathbf{M} , and \mathbf{M}_1 at the switching angular frequencies ω_l ($l = 1, 2, \dots, n$). Based on (8), the fitness of each individual in the secondary layer can be evaluated for the check of the second terminated conditions. If the secondary termination conditions are not satisfied, the algorithm goes to the operations of the adaptive mutation, the adaptive crossover, and the selection, to generate a new population for a further run of the secondary layer. On the contrary, if the secondary termination conditions are satisfied, the algorithm output the identified parameters of the equivalent resistances of the receiving resonators and the mutual inductances.

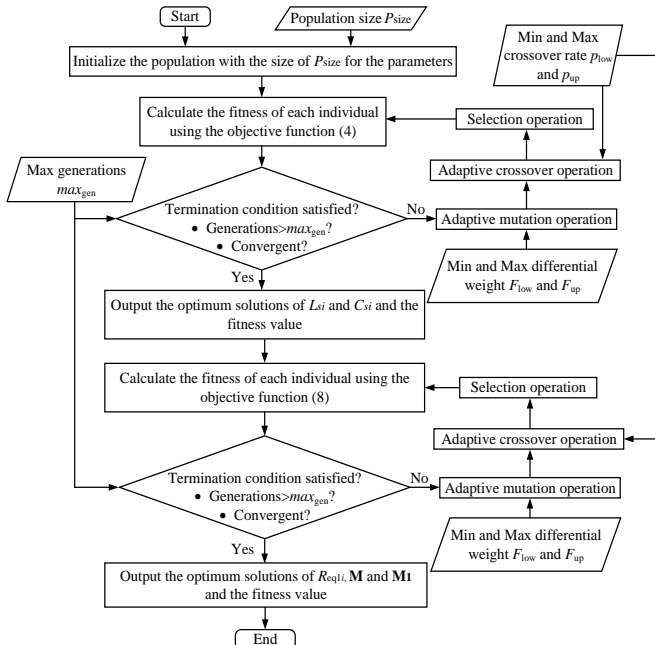


Fig. 3. Flowchart of the proposed two-layer ADE.

IV. EXPERIMENTAL VERIFICATION

Experiments are carried out on both two- and three-coil SS-compensated WPT systems, as shown in Fig. 4. To demonstrate the general applicability of the heuristic algorithms to accurately monitor the parameters of SS-compensated WPT systems, the coil dimensions are not optimized. The transmitting coils of both systems are 11 turns with the diameters of 31 cm. The receiving coil of the two-coil system is 11 turns with the diameter of 31 cm. Both the receiving coils of the three-coil systems are 11 turns with the diameters of 20 cm.

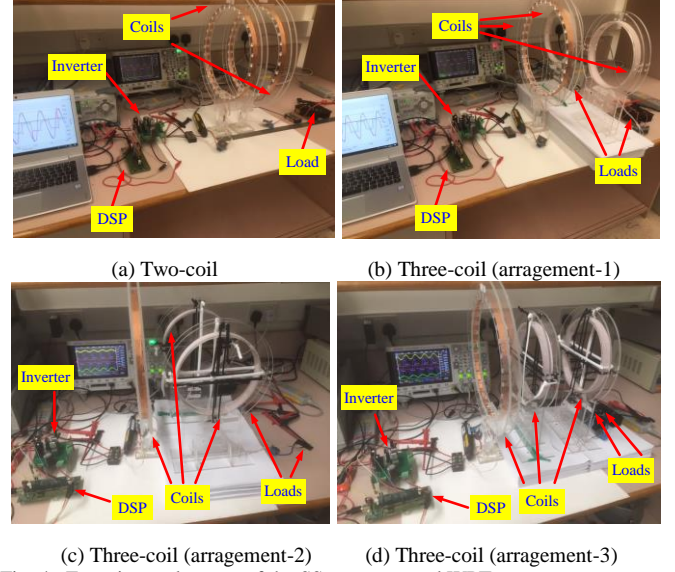


Fig. 4. Experimental setups of the SS-compensated WPT systems.

The schematic diagram of the three-coil SS-compensated WPT systems are depicted in Fig. 5. Fig. 5(a) shows the main circuit of the systems (For the two-coil system, only one load R_L is adopted), where the input voltage and current of the transmitting resonator, v_p and i_p , are measured. Fig. 5(b) shows the isolators and drivers used for the full-bridge inverter. Both v_p and i_p are measured by the oscilloscope InfiniiVision DSOX3024T and transmitted to Matlab via National Instrument's VISA. Fig. 5(c) shows the strategy of deriving the complex form of the fundamental components, v_{p1} and i_{p1} , from the measured v_p and i_p . The second-order bandpass filters are designed as

$$H(s) = \frac{2\zeta\omega_0 s}{s^2 + 2\zeta\omega_0 s + \omega_0^2} \quad (9)$$

where the damping ratio ζ is 0.05 for all the experiments. The complex values of \mathbf{i}_{p1} are used to calculate \mathbf{v}_{p1est} based on (2), which are further adopted to monitor the parameters of the SS-compensated WPT systems using the conventional GA, the ADE, and the two-layer ADE with the measured \mathbf{v}_{p1} in Matlab (For the two-layer ADE, \mathbf{v}_{p1} are used to calculate \mathbf{i}_{p1est} based on (8) for the secondary layer). The switching signals PWM1, PWM2, PWM3, and PWM4 are provided by a DSP of Texas Instruments' TMS320F28335 with fixed duty ratio of 0.5. The parameters of the resonators are accurately measured by an Agilent E5061B Network Analyzer, which are listed in Table I (Tx: transmitting resonator; Rx: receiving resonator of the two-coil system; Rx1: receiving resonator 1 of the three-coil system; Rx2: receiving resonator 2 of the three-coil system). All the compensated capacitors are designed to compensate the

self-inductances of the coils around the resonant frequency of 100 kHz.

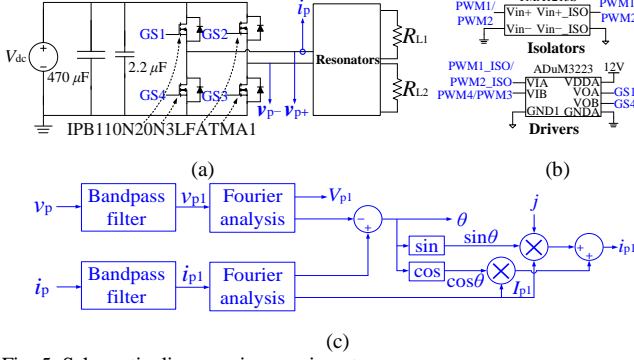


Fig. 5. Schematic diagrams in experiment.

TABLE I. PARAMETERS OF THE RESONATORS

Description	Symbol	Value
The inductance of the Tx	L_p	91.78 μH
The capacitance of the Tx	C_p	27.62 nF
The ESR of the Tx	R_p	0.7 Ω
The inductance of the Rx	L_s	92.05 μH
The capacitance of the Rx	C_s	27.2 nF
The ESR of the Rx	R_s	1.01 Ω
The inductance of the Rx1	L_{s1}	48.3 μH
The capacitance of the Rx1	C_{s1}	52.38 nF
The ESR of the Rx1	R_{s1}	0.24 Ω
The inductance of the Rx2	L_{s2}	48.8 μH
The capacitance of the Rx2	C_{s2}	51.18 nF
The ESR of the Rx2	R_{s2}	0.26 Ω

A. Two-Coil SS-Compensated WPT Systems

For the two-coil SS-compensated WPT system, the DC voltage source is 5 V and the switching frequency sweeps from 90 kHz to 110 kHz with the interval of 1 kHz. The distance between the coils D are changed from 10 cm to 20 cm with the interval of 2 cm. The corresponding mutual inductances are preliminarily measured, which are listed in Table II.

TABLE II. DISTANCES AND THE CORRESPONDING MUTUAL INDUCTANCE

D (cm)	M (μH)	D (cm)	M (μH)	D (cm)	M (μH)
10	15.515	14	10.194	18	7.021
12	12.333	16	8.431	20	5.935

The comparisons between the waveforms of v_p and i_p measured in the oscilloscope (Fig.6(a)-(c)) and v_p and i_p obtained in Matlab via National Instruments' VISA (Fig. 6(d)-(f)) for two-coil SS-compensated WPT systems with $R_L=10 \Omega$ and $D=10$ cm at the switching frequency of 90 kHz, 100 kHz (resonant frequency), and 110 kHz are shown in Fig. 6. Obviously, the waveforms obtained in Matlab are identical to the waveforms measured in the oscilloscope. The corresponding waveforms of the fundamental components of v_{p1} and i_{p1} , and the peak values of V_{p1} and I_{p1} are shown in Fig. 6(d)-(f). The fundamental components are well-extracted. The peak values are accurately measured.

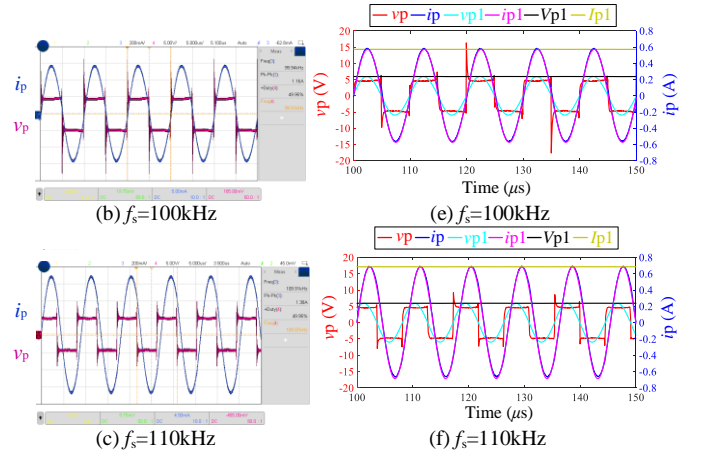
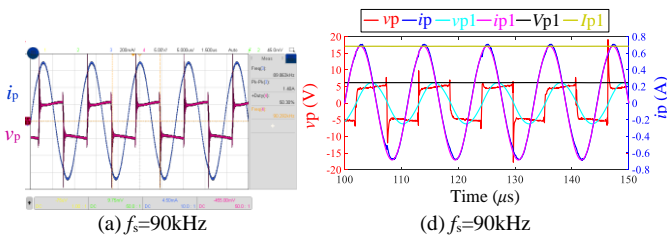


Fig. 6. Measured waveforms of two-coil SS-compensated WPT systems with $R_L=10 \Omega$ and $D=10$ cm.

TABLE III. CONSTRAINTS OF THE PARAMETERS FOR 2-COIL SYSTEMS

Lower bounds	Value	Upper bounds	Value
L_{sL}	80 μH	L_{sH}	100 μH
C_{sL}	20 nF	C_{sH}	50 nF
R_{eq1L}	0 Ω	R_{eq1H}	12 Ω
M_L	5 μH	M_H	20 μH

TABLE IV. PARAMETERS OF THE ALGORITHMS

Description	Symbol	Value
Chromosome size	C_{size}	10
Population size	P_{size}	64
Maximum generations	max_{gen}	2000
Crossover rate	P_c	0.26
Mutation rate	P_m	0.2
Lower bounds of the differential weight	F_{low}	0.1
Upper bounds of the differential weight	F_{up}	0.8
Lower bounds of the crossover rate	P_{low}	0.2
Upper bounds of the crossover rate	P_{up}	0.6
Lower bounds of the differential weight	F_{low}	0.1

The searching constraints of the monitored parameters L_s , C_s , R_{eq1} , and M are identically designed for the conventional GA, the ADE, and the two-layer ADE, as listed in Table III. The parameters of the algorithms are given in Table IV. In this paper, the parameters of the secondary layer of the two-layer ADE are identical to the parameters of the primary layer of the two-layer ADE.

1) Conventional GA

For $R_L=10 \Omega$ and $D=10$ cm, the parameters are monitored by the conventional GA ten times independently. The comparisons between the monitored and the actual parameters of L_s , C_s , R_{eq1} , and M , and their relative errors are shown in Fig. 7(a)-(d), respectively. Despite the relative errors of the monitored L_s and C_s by the conventional GA are within 5%, the variations are significant. For the relative errors of the monitored R_{eq1} and M , the relative errors can be greater than 10% and the variations are significant as well. Furthermore, the conventional GA are adopted to monitor the parameters for the other 11 cases of R_L and D . The 12 investigated cases are (Case 1~6: $R_L=10 \Omega$ and $D=10, 12, 14, 16, 18, 20$ cm; Case 7~12: $R_L=4.7 \Omega$ and $D=10, 12, 14, 16, 18, 20$ cm). The fitness values of the conventional GA for the 12 cases are depicted in Fig. 8. Apparently, the fitness values are unsteady, which exhibits the drawbacks of the conventional GA to find local optimal points. The maximum relative errors and the standard deviations of the parameters L_s ,

C_s , R_{eq1} , and M monitored by the conventional GA for the 12 cases are shown in Fig. 9. Due to the maximum relative errors of L_s and C_s are less than the maximum relative errors of R_{eq1} and M mostly, the monitoring performances of the conventional GA for L_s and C_s are better than the monitoring performances for R_{eq1} and M . However, the maximum relative error of L_s and C_s monitored by the conventional GA can still reach 11.09% and 10.01%. The maximum relative errors of R_{eq1} and M monitored by the conventional GA can reach 45.73% and 27.36%. The standard deviations of the monitored parameters are substantial. The percentages of the standard deviations over the actual values of the parameters can be 3.88%, 3.62%, 18.72%, and 8.24%, respectively, which reveals the uncertainties of the monitoring by the conventional GA.

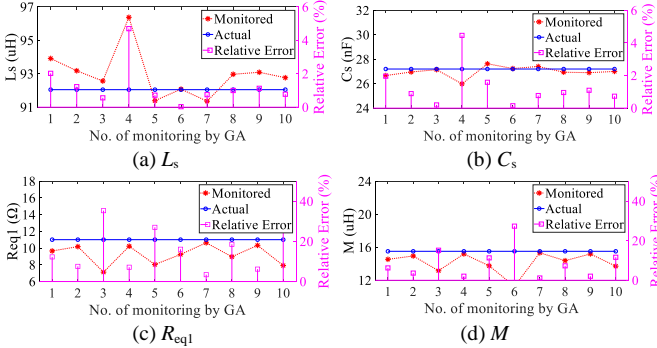


Fig. 7. Monitored results by the conventional GA for the two-coil SS-compensated WPT system with $R_L=10 \Omega$ and $D=10$ cm.

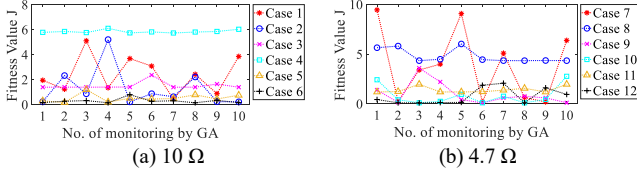


Fig. 8. Fitness values of the conventional GA for the 12 cases.

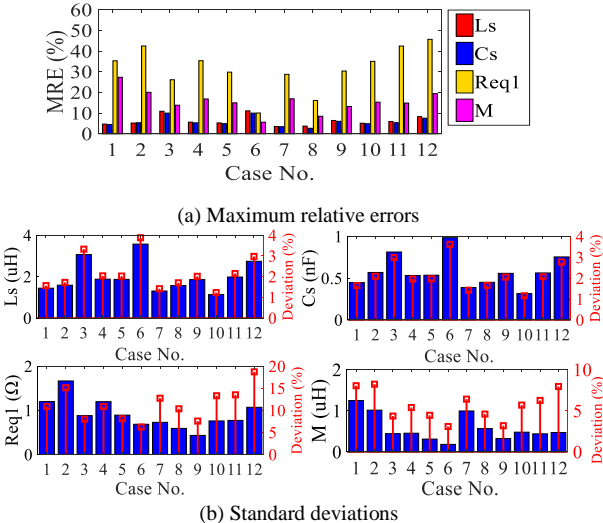


Fig. 9. Maximum relative errors and standard deviations of the parameters monitored by the conventional GA for the 12 cases

2) ADE

The parameters are monitored by the ADE with the population size of $P_{size}=7*nvar$. Here, $nvar$ indicates the number of the monitored variables. The maximum generations max_{gen} are tuned to implement fast convergence. For $R_L=10 \Omega$

and $D=10$ cm, the comparisons between the monitored and the actual parameters of L_s , C_s , R_{eq1} , and M , and their relative errors are shown in Fig. 10(a)-(d), respectively. Since the generations of the ADE converges at 233, the parameters of L_s , C_s , R_{eq1} , and M can be steadily monitored for the generations of 233, 500, 1000, and 2000. After the convergence, the relative errors of the monitored L_s , C_s , and M are less than 0.5% and the relative errors of the monitored R_{eq1} are less than 1%. The ADE are also adopted to monitor the parameters for the other 11 cases. The fitness values of the ADE for the 12 cases are depicted in Fig. 11. Obviously, these fitness values are steady after the convergence (233, 240, 200, 90, 250, 240, 250, 160, 200, 350, 230, 360 generations for cases 1-12), which validates the ADE can find global optimal points. The comparisons of the average relative errors and the standard deviations of the parameters L_s , C_s , R_{eq1} , and M monitored by the conventional GA and the ADE for all the 12 cases are shown in Fig. 12. Both the average relative errors and the standard deviations of the monitored parameters for the ADE are smaller than the ones for the conventional GA. The average relative errors of the monitored parameters for all the 12 cases can be reduced about 1% for L_s , 0.8% for C_s , 10.4% for R_{eq1} , and 4.6% for M . The standard deviations of the monitored parameters for all the 12 cases can be reduced about 42.01% for L_s , 40.75% for C_s , 78.84% for $R_{eq1}=10 \Omega$, 75.6% for $R_{eq1}=4.7 \Omega$, 83.42% for $M=15.515 \mu H$, 88.26% for $M=12.333 \mu H$, 78.87% for $M=10.194 \mu H$, 96.83% for $M=8.431 \mu H$, 90.91% for $M=7.021 \mu H$, and 98.35% for $M=5.935 \mu H$. Both results demonstrate that the ADE can monitor the parameters of two-coil SS-compensated WPT systems more steadily and accurately than the conventional GA.

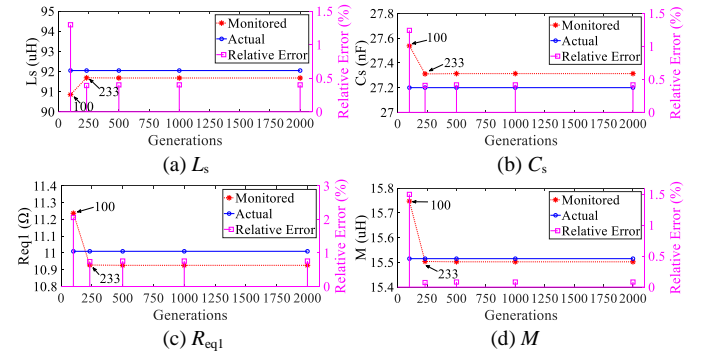


Fig. 10. Monitored results by the ADE for the two-coil SS-compensated WPT system with $R_L=10 \Omega$ and $D=10$ cm.

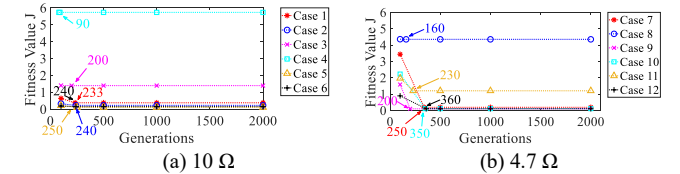


Fig. 11. Fitness values of the ADE for the 12 cases.

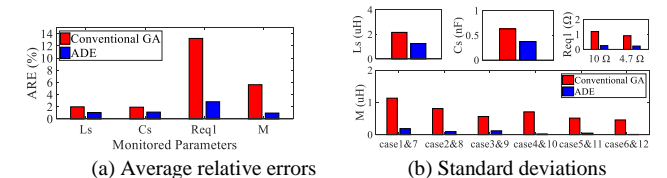


Fig. 12. Comparisons of the monitoring performances between the conventional GA and the ADE for all the 12 cases.

3) Two-Layer ADE

The population sizes of the two-layer ADE are tuned to be $P_{size}=5*nvar$ for both layers of optimization. For all the 12 cases of two-coil SS-compensated WPT systems, the fitness values of the two-layer ADE equalize the fitness values of the ADE. The comparisons of the average relative errors and the standard deviations of the monitored parameters between the ADE and the two-layer ADE are shown in Fig. 13. The results reveal that the monitoring performances of the two-layer ADE are almost the same as the ADE for two-coil SS-compensated WPT systems (the improvements are less than 1%).

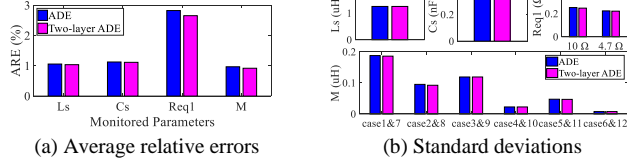


Fig. 13. Comparisons of the monitoring performances between the ADE and the two-layer ADE for the 12 cases.

B. Three-Coil SS-Compensated WPT Systems

For the three-coil SS-compensated WPT system, the DC voltage source V_{dc} is 5 V, while the switching frequency sweeps from 90 kHz to 98 kHz with the interval of 1 kHz, 98 kHz to 102 kHz with the interval of 0.2 kHz, and 102 kHz to 110 kHz with the interval of 1 kHz. Three arrangements of the three-coil WPT systems are plotted in Fig. 14.

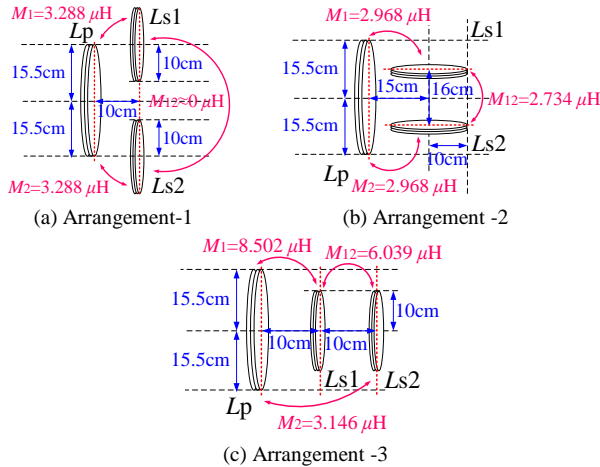


Fig. 14. Arrangements of the coils in three-coil WPT systems.

1) Arrangement-1

For arrangement-1, the mutual inductances between the transmitting coil and the receiving coils are 3.288 μ H (i.e., $M_1=M_2=3.288 \mu$ H), while the mutual inductance between the two receiving coils is negligible (i.e., $M_{12}\approx 0 \mu$ H). The comparisons between the waveforms of v_p and i_p measured in the oscilloscope (Fig.15(a)-(c)) and v_p and i_p obtained in Matlab via VISA (Fig. 15(d)-(f)) for three-coil SS-compensated WPT systems with arrangement-1 and $R_{L1}=R_{L2}=10 \Omega$ at the switching frequency of 90 kHz, 100 kHz (resonant frequency), and 110 kHz are shown in Fig. 15. The fundamental components are well-extracted and the peak values of v_{p1} and i_{p1} are accurately measured.

The three heuristic algorithms (i.e., GA, ADE, and the two-layer ADE) are adopted to monitor the parameters of three-coil SS-compensated WPT systems with arrangement-1 and four different load conditions (Case 13: $R_{L1}=R_{L2}=10 \Omega$,

Arrangement-1; Case 14: $R_{L1}=10 \Omega$ and $R_{L2}=4.7 \Omega$, Arrangement-1; Case 15: $R_{L1}=4.7 \Omega$ and $R_{L2}=10 \Omega$, Arrangement-1; Case 16: $R_{L1}=R_{L2}=4.7 \Omega$, Arrangement-1). The searching constraints of the monitored parameters L_{s1} , L_{s2} , C_{s1} , C_{s2} , R_{eq11} , R_{eq12} , M_1 and M_2 are listed in Table V. The parameters of the three algorithms are the same as the parameters for the two-coil systems.

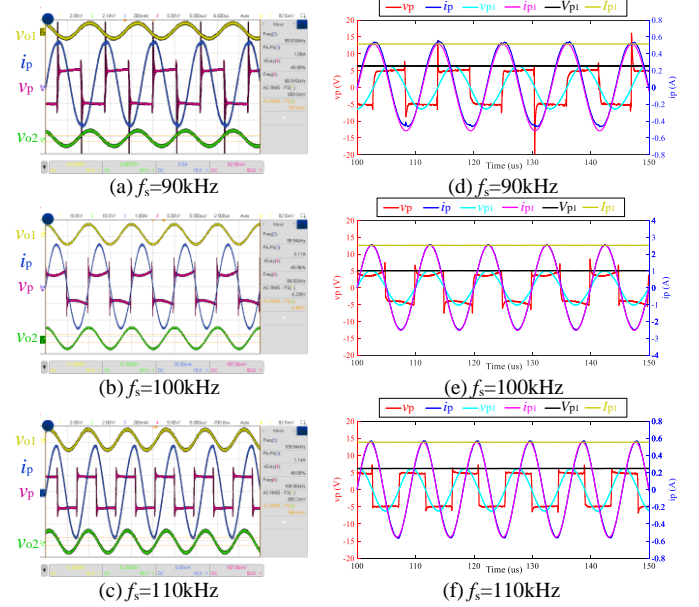


Fig. 15. Measured waveforms of the three-coil SS-compensated WPT systems with arrangement-1 and $R_{L1}=R_{L2}=10 \Omega$.

TABLE V. CONSTRAINTS OF THE PARAMETERS WITH ARRANGEMENT-1

Lower bound	Value	Upper bound	Value
L_{s1L}	45 μ H	L_{s1H}	55 μ H
L_{s2L}	45 μ H	L_{s2H}	55 μ H
C_{s1L}	40 nF	C_{s1H}	60 nF
C_{s2L}	40 nF	C_{s2H}	60 nF
R_{eq11L}	2 Ω	R_{eq11H}	12 Ω
R_{eq12L}	2 Ω	R_{eq12H}	12 Ω
M_{1L}	1 μ H	M_{1H}	5 μ H
M_{2L}	1 μ H	M_{2H}	5 μ H

The fitness values of the three algorithms for the cases 13~16 are presented in Fig. 16. The conventional GA is conducted ten times independently. The fitness values of the conventional GA vary frequently and do not converge at the global optimum. For the ADE, the algorithm converges at 420, 2700, 1850, and 1000 generations for the cases 13~16, respectively. For the secondary layer of the two-layer ADE, the algorithm converges at 420, 1660, 1800, 1500 generations for the cases 13~16, respectively.

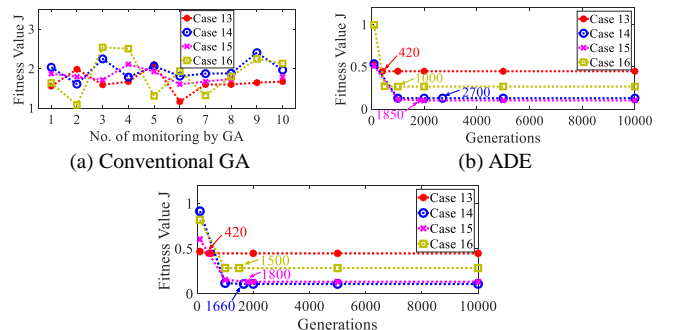


Fig. 16. Fitness values of the three algorithms for the cases 13~16.

The comparisons of the maximum relative errors, the average relative errors, and the standard deviations of the monitored parameters identified by the three heuristic algorithms for the cases 13~16 are shown in Fig. 17. All the maximum relative errors, the average relative errors and the standard deviations of the monitored parameters can be significantly reduced by adopting the ADE instead of the conventional GA. The maximum relative errors of the monitored parameters can be reduced about 43.31% for L_{s1} , 80.47% for C_{s1} , 42.95% for R_{eq11} , 80.92% for M_1 , 41.98% for L_{s2} , 93.87% for C_{s2} , 57.17% for R_{eq12} , and 80.87% for M_2 . The average relative errors of the monitored parameters can be reduced about 33.38% for L_{s1} , 53.42% for C_{s1} , 64.77% for R_{eq11} , 94.85% for M_1 , 22.52% for L_{s2} , 51.73% for C_{s2} , 80.09% for R_{eq12} , and 94.94% for M_2 . The standard deviations of the monitored parameters can be reduced about 92.53% for L_{s1} , 90.22% for L_{s2} , 97.79% for C_{s1} , 98.19% for C_{s2} , 95.71% for M_1 , 93.97% for M_2 , and nearly 99.9% for the loads of cases 13~16. The results demonstrate that the ADE can monitor the parameters of three-coil SS-compensated WPT system with arrangement-1 more steadily and accurately than the conventional GA. Besides, the standard deviations of the monitored parameters by the ADE and the two-layer ADE are approximately equal, which indicates the stabilities of both algorithms can be guaranteed. However, the maximum relative errors and the average relative errors of the monitored R_{eq11} and R_{eq12} for the two-layer ADE can be remarkably reduced about 79.63% and 85.52% for R_{eq11} and 66.51% and 77.01% for R_{eq12} , as compared to the ADE. The maximum relative errors of the monitored L_{s1} , L_{s2} , and C_{s2} are almost identical. The maximum relative errors of the monitored C_{s1} , M_1 , and M_2 can be decreased about 18.57% for C_{s1} and 26.15% for both M_1 and M_2 . In addition, the average relative errors of monitored parameters can be reduced about 9.43% for L_{s1} , 8.76% for C_{s1} , 8.69% for L_{s2} , 7.33% for C_{s2} , and 16.34% for both M_1 and M_2 by adopting the two-layer ADE instead of the ADE. Apparently, the two-layer ADE can further improve the accuracy of monitoring for the three-coil SS-compensated WPT system with arrangement-1.

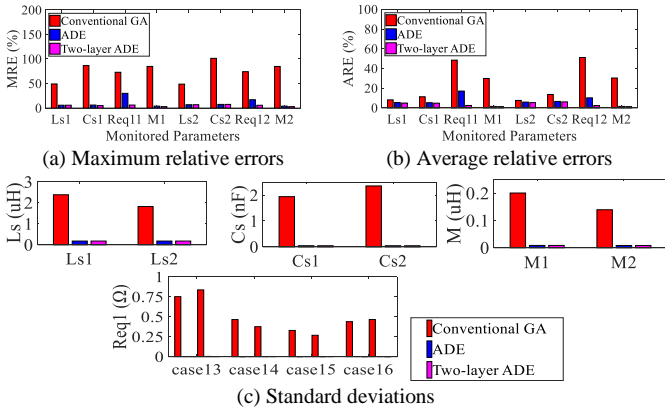


Fig. 17. Comparisons of the monitoring performance among the three algorithms for the cases 13~16.

2) Arrangement-2

For arrangement-2, the mutual inductances between the transmitting coil and the receiving coils are $2.968 \mu\text{H}$ (i.e., $M_1=M_2=2.968 \mu\text{H}$) and the mutual inductance between the two receiving coils is $2.734 \mu\text{H}$ (i.e., $M_{12}=2.734 \mu\text{H}$). The three

algorithms are adopted to monitor the parameters of three-coil SS-compensated WPT systems with four different load conditions (**Case 17: $R_{L1}=R_{L2}=10 \Omega$, Arrangement-2; Case 18: $R_{L1}=10 \Omega$ and $R_{L2}=4.7 \Omega$, Arrangement-2; Case 19: $R_{L1}=4.7 \Omega$ and $R_{L2}=10 \Omega$, Arrangement-2; Case 20: $R_{L1}=R_{L2}=4.7 \Omega$, Arrangement-2**). The searching constraints of the monitored parameters L_{s1} , L_{s2} , C_{s1} , C_{s2} , R_{eq11} , R_{eq12} , M_1 and M_2 are the same as the constraints in Table V. The lower bound and the upper bound of M_{12} are $1 \mu\text{H}$ and $10 \mu\text{H}$, respectively. The parameters of the three algorithms are the same as the parameters for the two-coil systems.

The fitness values of the three algorithms for the cases 17~20 are presented in Fig. 18. The fitness values of the conventional GA do not converge at the global optimum. The fitness values of the ADE converge at 450, 3120, 1920, and 880 generations for the cases 17~20, respectively. The fitness values of the secondary layer of the two-layer ADE converge at 450, 2200, 1900, and 1630 generations for the cases 17~20, respectively.

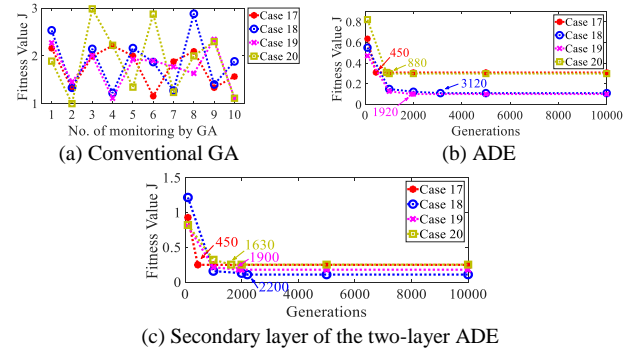


Fig. 18. Fitness values of the three algorithms for the cases 17~20.

The comparisons of the maximum relative errors, the average relative errors, and the standard deviations of the monitored parameters identified by the three heuristic algorithms for the cases 17~20 are shown in Fig. 19. Compare the ADE to the conventional GA, the maximum relative errors of the monitored parameters can be reduced about 88.91% for L_{s1} , 90.16% for C_{s1} , 55.24% for R_{eq11} , 92.63% for M_1 , 88.78% for L_{s2} , 90.64% for C_{s2} , 60.3% for R_{eq12} , 92.98% for M_2 and 89.09% for M_{12} . The average relative errors of the monitored parameters can be reduced about 20.39% for L_{s1} , 41.9% for C_{s1} , 65.64% for R_{eq11} , 93.02% for M_1 , 26.42% for L_{s2} , 33.33% for C_{s2} , 80.03% for R_{eq12} , 92.01% for M_2 and 63.64% for M_{12} . The standard deviations of the monitored parameters can be reduced about 95% for L_{s1} , 91.67% for L_{s2} , 98.36% for C_{s1} , 98.81% for C_{s2} , 97.5% for M_1 , 97.37% for M_2 , 95.45% for M_{12} , and nearly 99% for the loads of cases 17~20. Apparently, ADE can monitor all the parameters, including the mutual inductance between the receiving coils (i.e., M_{12}), more steadily and accurately than the conventional GA for the three-coil SS-compensated WPT system with arrangement-2. Furthermore, for the two-layer ADE, the maximum relative errors and the average relative errors of R_{eq11} and R_{eq12} can be reduced about 76% and 48% for R_{eq11} and 74.22% and 64.75% for R_{eq12} , as compared to the ADE. The maximum relative errors of the monitored L_{s1} , L_{s2} , C_{s1} , and C_{s2} are almost identical. The maximum relative errors of the monitored M_1 , M_2 , and M_{12} can be reduced about 20.51% for M_1 , 9.33% for M_2 , and 50% for M_{12} . Additionally, the average relative errors of monitored parameters can be reduced about 4.88% for L_{s1} , 13.94% for C_{s1} ,

6.41% for L_{s2} , 11.76% for C_{s2} , 40% for M_1 , 48% for M_2 , and 25% for M_{12} by using the two-layer ADE rather than the ADE. Obviously, the two-layer ADE exhibits better monitoring accuracy than the ADE for the three-coil SS-compensated WPT system with arrangement-2.

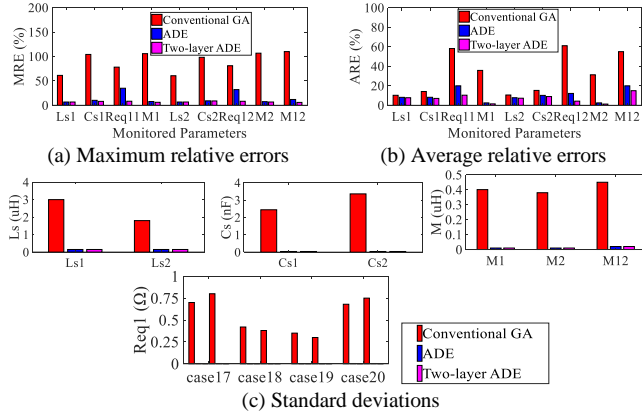


Fig. 19. Comparisons of the monitoring performance among the three algorithms for the cases 17~20.

3) Arrangement-3

For arrangement-3, the mutual inductances between the transmitting coil and the receiving coils are $8.502 \mu\text{H}$ and $3.146 \mu\text{H}$, respectively (i.e., $M_1=8.502 \mu\text{H}$ and $M_2=3.146 \mu\text{H}$) and the mutual inductance between the two receiving coils is $6.039 \mu\text{H}$ (i.e., $M_{12}=6.039 \mu\text{H}$). The three algorithms are adopted to monitor the parameters of three-coil SS-compensated WPT systems with four different load conditions (**Case 21: $R_{L1}=R_{L2}=10 \Omega$, Arrangement-3; Case 22: $R_{L1}=10 \Omega$ and $R_{L2}=4.7 \Omega$, Arrangement-3; Case 23: $R_{L1}=4.7 \Omega$ and $R_{L2}=10 \Omega$, Arrangement-3; Case 24: $R_{L1}=R_{L2}=4.7 \Omega$, Arrangement-3**). The searching constraints of the monitored parameters L_{s1} , L_{s2} , C_{s1} , C_{s2} , R_{eq11} , R_{eq12} , and M_2 are the same as the constraints in Table V. Both the lower bounds and the upper bounds of M_1 and M_{12} are $1 \mu\text{H}$ and $10 \mu\text{H}$, respectively. The parameters of the three algorithms are the same as the parameters for the two-coil systems.

The comparisons of the maximum relative errors, the average relative errors, and the standard deviations of the monitored parameters identified by the three heuristic algorithms for the cases 21~24 are shown in Fig. 20. Compare the ADE to the conventional GA, the maximum relative errors of L_{s1} , C_{s1} , R_{eq11} , L_{s2} , C_{s2} , R_{eq12} , M_1 , M_2 , and M_{12} are reduced about 92.59%, 95.03%, 82.4%, 91.9%, 94.54%, 80.05%, 87.22%, 90.67%, and 88.73%, respectively. The average relative errors are reduced about 44.09%, 38.73%, 88.4%, 32.56%, 39.81%, 80.69%, 88.61%, 86.93%, and 63.33%, respectively. The standard deviations are reduced about 95% for L_{s1} , 91.67% for L_{s2} , 98.36% for C_{s1} , 98.81% for C_{s2} , 97.05% for M_1 , 97.37% for M_2 , 95.45% for M_{12} , and nearly 99% for the loads of cases 21~24. The results demonstrate the ADE can monitor the parameters of the three-coil SS-compensated WPT system with arrangement-3 more accurately and steadily than the conventional GA. Compare the two-layer ADE to the ADE, the estimation errors of some parameters are further decreased. The maximum relative errors of R_{eq11} , R_{eq12} , M_1 , M_2 , and M_{12} are reduced about 55%, 50.42%, 52.94%, 32.1%, 51.39%, respectively. The average relative errors of L_{s1} , C_{s1} , R_{eq11} , L_{s2} ,

C_{s2} , R_{eq12} , M_1 , M_2 , and M_{12} are reduced about 19.23%, 18.4%, 42.86%, 25.86%, 19.35%, 46.77%, 33.33%, 45%, and 60%, respectively. The results validate the two-layer ADE can monitor the parameters of the three-coil SS-compensated WPT system with arrangement-3 more accurately than the ADE.

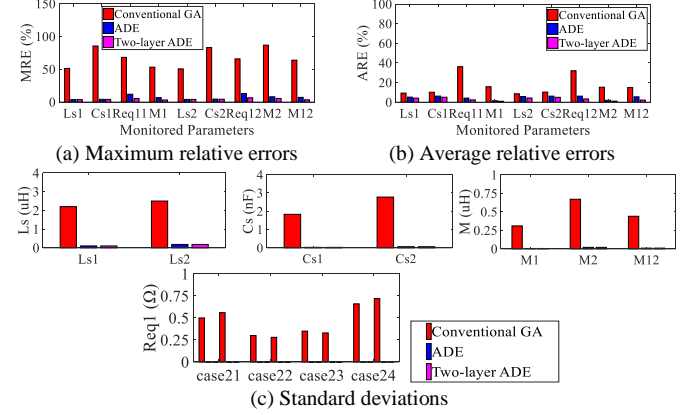


Fig. 20. Comparisons of the monitoring performance among the three algorithms for the cases 21~24.

C. Computation Time

The comparisons of computation time among the three algorithms are plotted in Fig. 21. The average computation time of the conventional GA, the ADE, and the two-layer ADE are 14.38s, 17.95s, and 33.77s for the two-coil WPT system. The computation time is increased about 3.57s from the conventional GA to the ADE. It is further increased about 15.82s from the ADE to the two-layer ADE. The average computation time of the three algorithms are 59.4s, 103.84s, and 192.53s for the three-coil WPT system with arrangement-1. They are 62.2s, 105.05s, and 195.73s for the three-coil WPT system with arrangement-2 and 60s, 95.47s, and 186.62s for the three-coil WPT system with arrangement-3. The average computation time of the three algorithms are 60.53s, 101.6s, and 191.63s for the three-coil WPT systems with three arrangements. The computation time is increased about 41.07s from the conventional GA to the ADE. It is further increased about 90.03s from the ADE to the two-layer ADE. Compared to the conventional GA and the ADE, the two-layer ADE takes longer time for both two-coil and three-coil WPT systems. However, due to the stability and accuracy are the primary concerns for the parameter monitoring, the two-layer ADE is preferred to monitor three-coil WPT systems. For two-coil WPT systems, the ADE is suggested to be used. This is because the ADE can monitor the parameters as the same accuracy as the two-layer ADE but takes much less computation time for the two-coil WPT systems. Besides, owing to the computation time are much shorter than the charging time of general WPT systems, both the ADE and the two-layer ADE can be adopted online for two-coil and three-coil SS-compensated WPT systems, respectively.

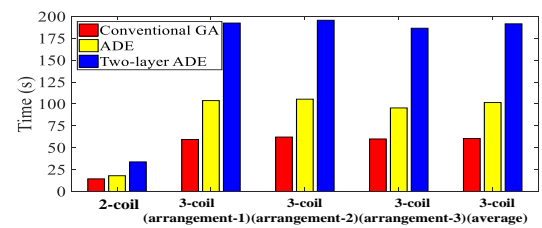


Fig. 21. Comparisons of the computation time among the three algorithms.

V. CONCLUSION

This paper presents an online front-end parameter monitoring method based on a two-layer ADE algorithm for SS-compensated WPT systems. The proposed two-layer ADE is compared to the conventional GA and the ADE for both two-coil and three-coil SS-compensated WPT systems. Experimental results validate that both the ADE and the proposed two-layer ADE can monitor the parameters of the receiving resonators and the mutual inductances much more steadily and accurately than the conventional GA for both two-coil and three-coil SS-compensated WPT systems. The ADE can monitor the parameters as the same accuracy as the two-layer ADE for the two-coil WPT systems. However, the two-layer ADE can monitor the parameters more accurately than the ADE for three-coil WPT systems. For the three-coil SS-compensated WPT systems with three different arrangements, the average relative errors of the monitored parameters can be reduced at the minimum of 4.88% and at the maximum of 60%. The computation time of the two-layer ADE is longer than that of the ADE. Therefore, the ADE is suggested to monitor the parameters of two-coil SS-compensated WPT systems and the two-layer ADE is suggested to monitor the parameters of three-coil SS-compensated WPT systems.

ACKNOWLEDGMENT

We would like to thank the support of Hong Kong Research Grant Council under Theme-based Research Project T23-701/14-N and the help from Ms. Hui Wen Rebecca Liang.

REFERENCES

- [1] N. Tesla, "Apparatus for transmitting electrical energy," U.S. Patent 1119732, Dec. 1, 1914.
- [2] S. C. Tang, T. L. T. Lun, Z. Guo, et al., "Intermediate range wireless power transfer with segmented coil transmitters for implantable heart pumps," *IEEE Tran. Power Electron.*, vol. 32, no. 5, pp. 3844–3857, May 2017.
- [3] S. C. Tang, "A low-operating-voltage wireless intermediate-range scheme for energy and signal transmission by magnetic coupling for implantable devices," *IEEE J. Emerg. Sel. Topics Power Electron.*, vol. 3, no. 1, pp. 242–251, Mar. 2015.
- [4] J. G. Bum and B. H. Cho, "An energy transmission system for an artificial heart using leakage inductance compensation of transcutaneous transformer," *IEEE Tran. Power Electron.*, vol. 13, no. 6, pp. 1013–1022, Nov. 1998.
- [5] J. Huh, S. W. Lee, W. Y. Lee, G. H. Cho, and C. T. Rim, "Narrow-width inductive power transfer system for online electrical vehicles," *IEEE Tran. Power Electron.*, vol. 26, no. 12, pp. 3666–3679, Dec. 2011.
- [6] G. A. Covic, J. T. Boys, M. L. G. Kissin, and H. G. Lu, "A three-phase inductive power transfer system for roadway-powered vehicles," *IEEE Trans. Ind. Electron.*, vol. 54, no. 6, pp. 3370–3378, Dec. 2007.
- [7] J. Sallán, J. L. Villa, A. Lombart, and J. F. Sanz, "Optimal design of ICPT systems applied to electric vehicle battery charge," *IEEE Tran. Ind. Electron.*, vol. 56, no. 6, pp. 2140–2149, Jun. 2009.
- [8] W. G. Hurley and J. Kassakian, "Induction heating of circular ferromagnetic plates," *IEEE Tran. Magn.*, vol. 15, no. 4, pp. 1174–1181, Jul. 1979.
- [9] S. Y. R. Hui, "Planar inductive battery charging system," U.S. Patent 7576514, Aug. 18, 2009.
- [10] S. Y. R. Hui and W. C. Ho, "A new generation of universal contactless battery charging platform for portable consumer electronic equipment," *IEEE Tran. Power Electron.*, vol. 20, no. 3, pp. 620–627, May 2005.
- [11] X. Liu and S. Y. R. Hui, "Simulation study and experimental verification of a contactless battery charging platform with localized charging features," *IEEE Tran. Power Electron.*, vol. 22, no. 6, pp. 2202–2210, Nov. 2007.
- [12] B. Choi, J. Nho, H. Cha, T. Ahn and S. Choi, "Design and implementation of low-profile contactless battery charger using planar printed circuit board windings as energy transfer device," *IEEE Tran. Ind. Electron.*, vol. 51, no. 1, pp. 140–147, Feb. 2004.
- [13] Y. Jang and M. M. Jovanovic, "A contactless electrical energy transmission system for portable-telephone battery chargers," *IEEE Tran. Ind. Electron.*, vol. 50, no. 3, pp. 520–527, Jun. 2003.
- [14] C.-G. Kim, D.-H. Seo, J.-S. You, J.-H. Park, and B. H. Cho, "Design of a contactless battery charger for cellular phone," *IEEE Tran. Ind. Electron.*, vol. 48, no. 6, pp. 1238–1247, Dec. 2001.
- [15] X. Qu, Y. Jing, H. Han, S. C. Wong, and C. K. Tse, "Higher order compensation for inductive-power-transfer converters with constant-voltage or constant-current output combating transformer parameter constraints," *IEEE Tran. Power Electron.*, vol. 32, no. 1, pp. 394–405, Jan. 2017.
- [16] W. Zhang and C. C. Mi, "Compensation topologies of high-power wireless power transfer systems," *IEEE Trans. Vehicular Electron.*, vol. 30, no. 11, pp. 6434–6445, Feb. 2015.
- [17] H. Li, K. Wang, J. Fang, and Y. Tang, "Pulse density modulated ZVS for full-bridge converters for wireless power transfer systems," *IEEE Tran. Power Electron.*, vol. 34, no. 1, pp. 369–377, Jan. 2019.
- [18] X. Dai, X. Li, Y. Li, and A. P. Hu, "Maximum efficiency tracking for wireless power transfer systems with dynamic coupling coefficient estimation," *IEEE Tran. Power Electron.*, vol. 33, no. 6, pp. 5005–5015, Jun. 2018.
- [19] M. Fu, H. Yin, X. Zhu, and C. Ma, "Analysis and tracking of optimal load in wireless power transfer systems," *IEEE Tran. Power Electron.*, vol. 30, no. 7, pp. 3952–3963, Aug. 2014.
- [20] E. Gati, G. Kampitsis, and S. Manias, "Variable frequency controller for inductive power transfer in dynamic conditions," *IEEE Tran. Power Electron.*, vol. 32, no. 2, pp. 1684–1696, Feb. 2017.
- [21] W. X. Zhong and S. Y. R. Hui, "Maximum energy efficiency tracking for wireless power transfer systems," *IEEE Tran. Power Electron.*, vol. 30, no. 7, pp. 4025–4034, Feb. 2015.
- [22] Z. Huang, S. C. Wong, and C. K. Tse, "Control design for optimizing efficiency in inductive power transfer systems," *IEEE Tran. Power Electron.*, vol. 33, no. 5, pp. 4523–4534, May 2018.
- [23] R. Mai, Y. Liu, Y. Li, et al., "An active-rectifier-based maximum efficiency tracking method using an additional measurement coil for wireless power transfer," *IEEE Tran. on Power Electron.*, vol. 33, no. 1, pp. 716–728, Jan. 2018.
- [24] Z. Li, K. Song, J. Jiang, and C. Zhu, "Constant current charging and maximum efficiency tracking control scheme for supercapacitor wireless charging," *IEEE Tran. on Power Electron.*, vol. 33, no. 10, pp. 9088–9100, Oct. 2018.
- [25] H. L. Li, A. P. Hu, G. A. Covic, and C. Tang, "A new primary power regulation method for contactless power transfer," in *Proc. IEEE Int. Conf. Ind. Technol.*, Feb. 2009, pp. 1–5.
- [26] Y. Yang, W. Zhong, S. Kiratipongvoot, S. C. Tan, and S. Y. R. Hui, "Dynamic improvement of series-series compensated wireless power transfer systems using discrete sliding mode control," *IEEE Tran. on Power Electron.*, vol. 33, no. 7, pp. 6351–6360, Jul. 2018.
- [27] N. Y. Kim, K. Y. Kim, J. Choi, and C. W. Kim, "Adaptive frequency with power-level tracking system for efficient magnetic resonance wireless," *Electron. Lett.*, vol. 48, no. 8, pp. 452–454, Apr. 2012.
- [28] O. C. Onar, J. M. Miller, S. L. Campbell, C. Coomer, C. P. White, and L. E. Seiber, "Oak ridge national laboratory wireless power transfer development for sustainable campus initiative," in *Proc. IEEE Transp. Electrification Conf. Expo.*, Jun. 2013, pp. 1–8.
- [29] A. Namadmalan, "Self-oscillating tuning loops for series resonant inductive power transfer systems," *IEEE Tran. Power Electron.*, vol. 31, no. 10, pp. 7320–7327, Oct. 2016.
- [30] Z. Wang, Y. Li, Y. Sun, C. Tang, and X. Lv, "Load detection model of voltage-fed inductive power transfer system," *IEEE Tran. Power Electron.*, vol. 28, no. 11, pp. 5233–5243, Nov. 2013.
- [31] Y. Yang, Y. Jiang, S. C. Tan, and S. Y. R. Hui, "A frequency-sweep based load monitoring method for weakly-coupled series-series compensated wireless power transfer systems," in *PELS Workshop on Emerging Technologies: Wireless Power Transfer (WoW)*, Montréal, QC, Canada, Jun. 2018, pp. 1–5.
- [32] J. Yin, D. Lin, C. K. Lee, T. Parisini, and S. Y. R. Hui, "Front-end monitoring of multiple loads in wireless power transfer systems without wireless communication systems," *IEEE Tran. Power Electron.*, vol. 31, no. 3, pp. 2510–2517, Mar. 2016.
- [33] D. Lin, J. Yin, and S. Y. R. Hui, "Parameter identification of wireless power transfer systems using input voltage and current," in *IEEE Energy Conversion Congress and Exposition (ECCE)*, 2014, pp. 832–836.

- [34] S. N. Sivanandam and S. N. Deepa, *Principles of Soft Computing*, Wiley India Pvt. Limited, 2007.
- [35] D. Whitley, *A Genetic Algorithm Tutorial*, Statistics and Computing, 1994, 4(2), pp. 65–85.
- [36] J. Holland, *Adaptation in Nature and Artificial Systems*, University of Michigan Press, Ann Arbor, 1975.
- [37] R. Storn and K. Price, “Differential evolution – a fast and efficient heuristic for global optimization over continuous spaces,” *Journal of Global Optimization*, 1997.
- [38] T. Tušar and B. Filipič, “Differential evolution versus genetic algorithm in multi-objective optimization,” in *International Conference on Evolutionary Multi-Criterion Optimization*, 2007, pp. 257–271.
- [39] S. Das and P. N. Suganthan, “Differential evolution: a survey of the state-of-art,” *IEEE Tran. Evol. Comput.*, vol. 15, no. 1, pp. 4–31, Feb. 2011.
- [40] L. M. Zheng, S. X. Zhang, S. Y. Zheng, “Differential evolution algorithm with two-step subpopulation strategy and its application in microwave circuit designs,” *IEEE Tran. Ind. Inform.*, vol. 12, no. 3, pp. 911–923, Jun. 2016.
- [41] J. H. Zhong, M. Shen, J. Zhang, “A differential evolution algorithm with dual populations for solving periodic railway timetable scheduling problem,” *IEEE Tran. Evol. Comput.*, vol. 17, no. 4, pp. 512–527, Aug. 2013.
- [42] A. Bhattacharya and P. K. Chattopadhyay, “Hybrid differential evolution with biogeography-based optimization for solution of economic load dispatch,” *IEEE Tran. Power Syst.*, vol. 25, no. 4, pp. 1955–1964, Nov. 2010.
- [43] Y. Mao, S. X. Niu and Y. Yang, “Differential evolution-based multiobjective optimization of the electrical continuously variable transmission system,” *IEEE Tran. Ind. Electron.*, vol. 65, no. 3, pp. 2080–2089, Mar. 2018.
- [44] J. Brest, S. Greiner, B. Boskovic, M. Mernik, and V. Zumer, “Self-adapting control parameters in differential evolution: a comparative study on numerical benchmark problems,” *IEEE Tran. Evol. Comput.*, vol. 10, no. 6, pp. 646–657, Dec. 2006.



Yun Yang (M’18) received the B.S. degree in electrical engineering from Wuhan University, Wuhan, China, in 2012 and Ph.D. degree in power electronics from Department of Electrical and Electronic Engineering, The University of Hong Kong, Hong Kong, in 2017. He is currently a Postdoctoral Research Fellow in the Department of Electrical and Electronic Engineering, The University of Hong Kong. He has published more than 20 technical papers. He won the outstanding presentation award in APEC 2016 and served as a session chair in IEEE PELS Workshop on Emerging Technologies: Wireless Power 2018. His current research interests include power electronics and control, microgrids, and wireless power transfer.



Siew-Chong Tan (S’00–M’06–SM’11) received the B.Eng. (Hons.) and M.Eng. degrees in electrical and computer engineering from the National University of Singapore, Singapore, in 2000 and 2002, respectively, and the Ph.D. degree in electronic and information engineering from the Hong Kong Polytechnic University, Hong Kong, in 2005. He is currently a Professor in Department of Electrical and Electronic Engineering. Prof. Tan is an Associate Editor of the IEEE Transactions on Power Electronics. He is a coauthor of the book *Sliding Mode Control of Switching Power Converters: Techniques and Implementation* (Boca Raton: CRC, 2011). His research

interests are focused in the areas of power electronics and control, smart grids, and clean energy technologies.



Shu Yuen Ron Hui (M’87–SM’94–F’03) received his BSc (Eng) Hons at the University of Birmingham in 1984 and a D.I.C. and PhD at Imperial College London in 1987. Presently, he holds the Philip Wong Wilson Wong Chair Professorship at the University of Hong Kong and a Chair Professorship at Imperial College London.

He has published over 300 technical papers, including more than 220 refereed journal publications. Over 60 of his patents have been adopted by industry. He is an Associate Editor of the IEEE Transactions on Power Electronics and IEEE Transactions on Industrial Electronics, and an Editor of the IEEE Journal of Emerging and Selected Topics in Power Electronics. His inventions on wireless charging platform technology underpin key dimensions of Qi, the world’s first wireless power standard, with freedom of positioning and localized charging features for wireless charging of consumer electronics. He received the IEEE Rudolf Chope R&D Award from the IEEE Industrial Electronics Society and the IET Achievement Medal (The Crompton Medal) in 2010, and IEEE William E. Newell Power Electronics Award in 2015. He is a Fellow of the Australian Academy of Technological Sciences & Engineering (since 2010), the Royal Academy of Engineering, U.K (since 2016), and US Academy of Inventors (since 2018).